Applied Physics Letters

RESEARCH ARTICLE | APRIL 01 2024

Ferroelectric $Al_{1-x}B_xN$–GaN heterostructures

Joseph Casamento ; Fan He ; Chloe Skidmore ; John Hayden ; Josh Nordlander ; Joan M. Redwing ; Susan Trolier-McKinstry ; Jon-Paul Maria

Appl. Phys. Lett. 124, 142101 (2024)
https://doi.org/10.1063/5.0190556

30 April 2024 17:21:19

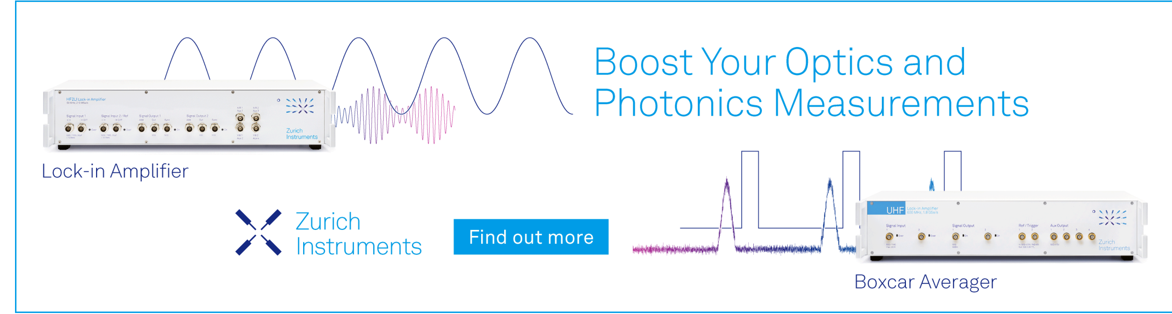

Applied Physics Letters ARTICLE pubs.aip.org/aip/apl

Ferroelectric $Al_{1-x}B_xN$–GaN heterostructures

Cite as: Appl. Phys. Lett. **124**, 142101 (2024); doi: 10.1063/5.0190556
Submitted: 6 December 2023 · Accepted: 21 February 2024 ·
Published Online: 1 April 2024

Joseph Casamento,[a] Fan He, Chloe Skidmore, John Hayden, Josh Nordlander, Joan M. Redwing, Susan Trolier-McKinstry, and Jon-Paul Maria

AFFILIATIONS

Department of Materials Science and Engineering, Materials Research Institute, Pennsylvania State University, University Park, Pennsylvania 16802, USA

[a]Author to whom correspondence should be addressed: jac5956@psu.edu

ABSTRACT

This report demonstrates $Al_{0.93}B_{0.7}N$ thin films grown epitaxially on n-type GaN (0002)/c-plane sapphire substrates by reactive magnetron sputtering at 300 °C. At 200 nm film thickness, the $Al_{0.93}B_{0.07}N$ layers exhibit partially relaxed substrate-induced epitaxial strain, a 0.16° wide (0002) rocking curve, in-plane crystallographic registry, and sub-nanometer surface roughness. Electrically, the stack shows robust hysteresis over three frequency decades, a remanent polarization of $\sim$125 μC/cm^2, a strongly frequency dependent coercive field, highly uniform dc leakage currents, and endurance $>10^6$ field cycles. This report validates possibilities for ferroelectric nitride integration into conventional III-nitride heterostructures with high crystalline fidelity, high electrical resistivity, and persistent hysteresis. Such materials are synthesizable at thermal budgets and temperatures compatible with back-end-of-the-line boundary conditions.

Published under an exclusive license by AIP Publishing. https://doi.org/10.1063/5.0190556

30 April 2024 17:21:19

Independently engineering semiconductor thin film microstructure, crystallinity, and resistivity most often introduces tradeoffs where optimizing one parameter comes at the expense of another, and where parameter tuning is thermodynamically limited. For example, metal organic chemical vapor deposition (MOCVD) produces crystals with superb crystalline fidelity and microstructure, but does so at growth temperatures typically >900 °C and conditions close to thermal equilibrium. This range exceeds GaN thermal decomposition conditions,[1,2] introducing challenges for defect chemistry control, for abrupt heteroepitaxial interfaces, and for solid solution stability in concentrated formulations.[3] Alternatively, reactive sputter deposition most often offers synthesis space far from equilibrium, with low substrate temperature and high adatom arrival energies. When properly controlled, these conditions are highly supersaturated and produce finer microstructures, better control of intrinsic defect chemistry, and potentially abrupt interfaces.[4] These positive aspects are typically accompanied by crystal perfection and/or epitaxy sacrifice. Currently, aluminum nitride-based acoustic wave devices and ferroelectric nitride capacitors containing Al,ScN and Al,BN are most commonly prepared by sputtering.[5,6] This stems in part from low deposition temperatures that are compatible with back end of line (BEOL) integration, with high available deposition rates that facilitate thicker resonant devices, and high supersaturation values that can produce defect chemistries offering high-field stability. Accordingly, ferroelectricity is demonstrated for these materials via sputtering on a variety of metal electrodes over a large thickness range.[7–10]

Current issues facing nitride ferroelectric technological adoption include large leakage current densities at the relatively large coercive fields (>3 MV/cm), the inability to thickness-scale below $\sim$50 nm without reduced insulation resistance, and a relative lack of endurance.[11] Current knowledge associates these challenges with: **i.** crystallographic and morphological transitions during the initial wurtzite nucleation from an elemental metal electrode surface, **ii.** chemical inhomogeneity and point defect chemistry close to the wurtzite nitride-metal electrode interface, and **iii.** defective interfaces that propagate defects (e.g., nitrogen vacancies) during multiple electrical measurement cycles.[12,13] Nitrogen vacancies, for example, are associated with decreasing effective Schottky barrier heights and increased electron tunneling.[14]

To address these issues and potentially circumvent the tradeoffs associated with sputter deposition on metal electrodes, doped GaN is an attractive substrate material. In principle, epitaxial growth on GaN should promote wurtzite phase formation and high crystalline fidelity at lower thickness values, it should favor the correct stoichiometry from the first monolayer, and it should trigger a growth mode (due to the isostructural template) that maximizes crystalline perfection, preserves surface smoothness, and generates abrupt internal interfaces. Additionally, since GaN is a foundation of nitride based transistors, power devices, light emitting diodes (LEDs), and lasers, integrating ferroelectric nitrides with it is a technological necessity. This approach was adopted for ferroelectric Al,ScN heterostructures grown by molecular beam epitaxy (MBE)[15–18] and in similar Al,ScN heterostructures via sputtering.[19,20] This report pursues these goals and expands upon

Published under an exclusive license by AIP Publishing

previous work by exploring an all-nitride, wurtzite ferroelectric Al,BN–GaN heterostructure at low deposition temperatures where the Al,BN layer is ~210 nm thick, and the bottom electrode is n-type doped semiconducting GaN on sapphire. The suite of structural, electrical, and morphological measurements demonstrates favorable combination of crystallinity, high-field stability, surface morphology, and polarization switching.

All Al,BN thin films discussed in this study are grown by reactive magnetron sputter deposition on metal polar n-type GaN–Al_2O_3 (0001) substrates. The n-type GaN layer is the epitaxial template and bottom electrode with a $3 \times 10^{18}/cm^3$ carrier density. Al,BN is deposited in 20 standard cubic centimeters per minute (sccm) of pure nitrogen (N_2) at 2 mTorr. Source materials include 2 in. Al (99.995% stated purity, Kurt J. Lesker) and 2 in. BN (99.5% stated purity, Plasmaterials) sputtering targets driven with pulsed DC (100 kHz, 1536 ns pulse width, 250 W time averaged power) and RF (13.56 MHz, 65 W time averaged power) power supplies, respectively. Lithographic liftoff of 100 nm thick room temperature deposited W films (dc-magnetron sputtered at 200 W, 2 in. target, 7 mTorr Ar) completes the parallel plate capacitor stacks.

Symmetric x-ray diffraction (XRD) $2\theta - \omega$ patterns and rocking curves are collected using a PANalytical Empyrean diffractometer with a Cu tube source. The incident optics include a Ge double bounce monochromator, a 1/8° divergence slit, a 1/2° antiscatter slit, and a 4 mm beam mask. The diffracted beam optics include a Pixcel3D detector, a 0.4 rad Soller slit, and 1/4° antiscatter slit. Surface morphology is characterized using an Asylum Research MFP3D atomic force microscopy (AFM) system in a tapping mode at a 270 kHz cantilever resonance frequency. Piezoresponse force microscopy (PFM) is performed with the same instrument in the contact mode. Polarization hysteresis loops are acquired with a PolyK ferroelectrics tester integrated with a Trek PDZ-350 amplifier. Ferroelectric fatigue measurements are collected on a Radiant Precision II Multiferroic system using a bipolar triangular voltage waveform. Polarization and fatigue testing are conducted at modest frequencies (<500 Hz) to ensure complete switching during each cycle. All measurements use a bottom-electrode-drive top-electrode-sense geometry.

Figure 1 provides an XRD and AFM summary of the Al,BN/GaN stack. The θ-2θ scan in Fig. 1(a) shows the GaN, AlN buffer layer, and

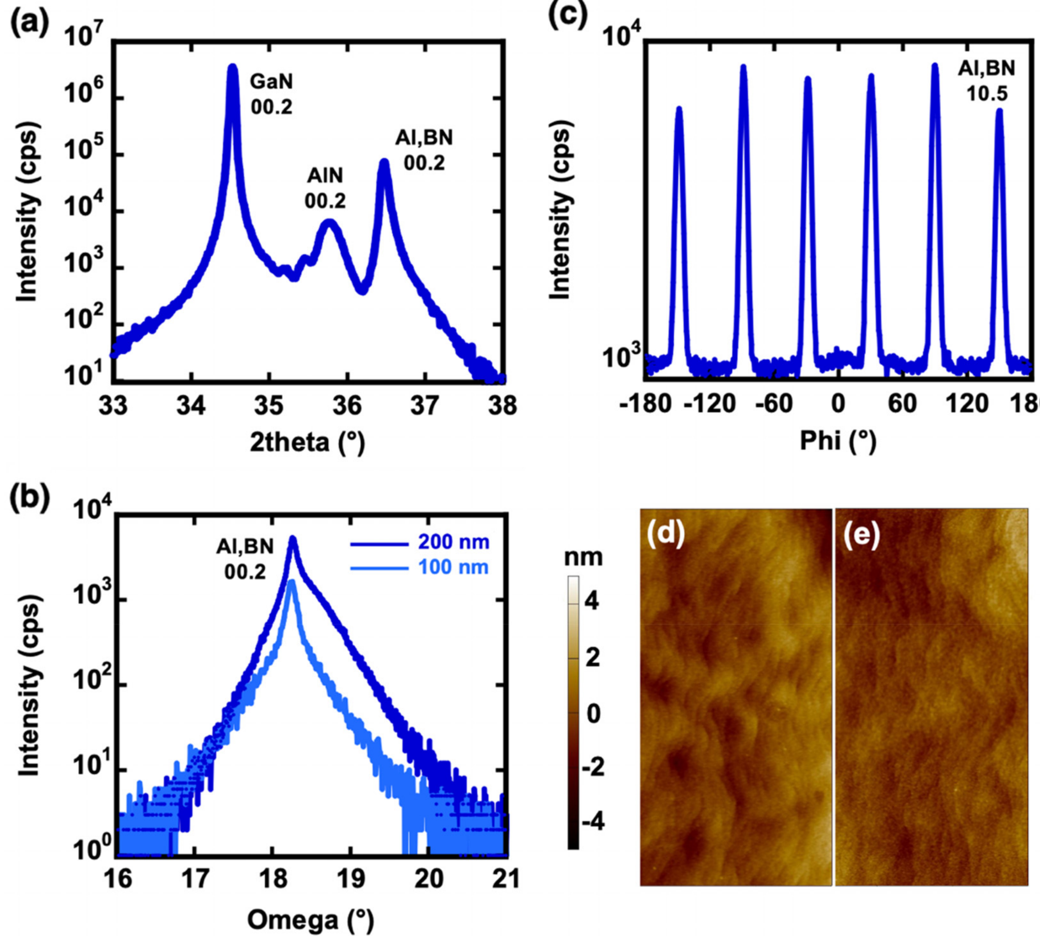

FIG. 1. (a) XRD θ-2θ scans showing the Al,BN thin film c-axis orientation, and the AlN peak is produced by the AlN nucleation layer on sapphire; (b) Al,BN 00.2 omega scan with a 0.16° FWHM. The logarithmic scale highlights the strain relaxation, (c) asymmetric Al,BN 10.5 ϕ-scan showing in-plane epitaxial registry to GaN, and (d) and (e) AFM topography images for 100 and 210 nm thick Al,BN films showing indications of step-and-terrace growth, respectively, and the AFM images have a 5 μm wide field of view.

30 April 2024 17:21:19

Published under an exclusive license by AIP Publishing

Al,BN (00.2) diffraction peaks and uniform *c*-axis orientation. The rocking curve in Fig. 1(b) has a full-width-half-maximum (FWHM) value of 0.16° indicating modest mosaicity—for context, the (00.2) GaN rocking curve FWHM is only marginally narrower at 0.12°. It is interesting to note the broader and lower intensity Al,BN rocking curve component that suggests a second crystallite population with more disorder. The two crystallite populations are also offset from each other in omega. Reimer *et al.*[21] explain that such patterns can originate from a near-interface layer that is coherently strained and perfectly aligned with the substrate, thus adopting whatever miscut is present, and a relaxed—and thus disordered—layer with mosaicity centered about the substrate physical normal. Figure 1(b) also contains rocking curve data for a 100 nm thick Al,BN layer prepared using identical conditions. Note the smaller FWHM of 0.14° and the reduced background intensity due to less relaxation. Overall, the mosaic spread is quite small considering the low growth temperature, and likely attributable to the considerable adatom kinetic energy during sputtering. Figure 1(a) shows an azimuthal scan of the Al,BN (10.5) planes, confirming in-plane lattice registry to the underlying GaN. Figures 1(d) and 1(e) show AFM tapping mode images of the 100 and 210 nm thick Al,BN film surfaces, respectively. The 100 nm film exhibits a step-and-terrace morphology, while the 210 nm film shows a partial transition to 3D growth. Such smooth surfaces, particularly at 100 nm, are noteworthy, given the 300 °C growth temperature. This suggests possibilities to integrate MOCVD, MBE, and sputtered nitrides without sacrificing crystalline and interfacial fidelity, at least in modest layer thicknesses.

Electrical properties of the heterostructure stacks are first explored by polarization hysteresis tests. Figure 2 shows the single-cycle P-E loops performed as a function of measurement frequency on Al,BN/GaN heterostructures. P-E loop measurements with clear saturation signatures are evident between 1 Hz and 1 kHz. Currently, these are among the lowest frequency loops reported and indicate high insulation resistance. With decreasing frequency, the remanent polarization is relatively constant ~125 μC/cm^2, and the coercive field decreases from ~6.1 MV/cm at 1 kHz to ~4 MV/cm at 1 Hz. While data for only one B concentration is shown here, as demonstrated elsewhere,[6] ferroelectric switching can be observed from 0% to 19% B. Ferroelectric coercive fields are strongly frequency dependent in systems where switching follows a nucleation and growth mechanism, and this appears in Al,BN as noted by Zhu *et al.*[7] and Yazawa *et al.*[22] The remanent polarization values increase slightly with reduced frequency, but this change reflects a larger leakage current contribution that can obscure the pure polarization reversal current. The data in Fig. 3 do not include leakage current corrections.

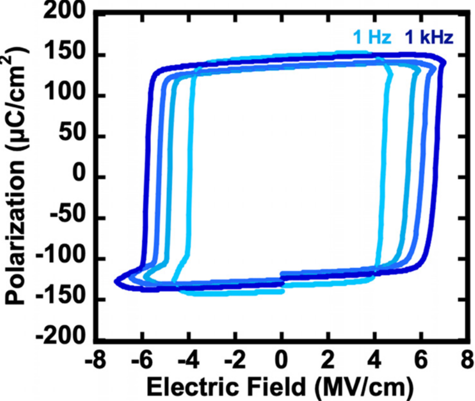

FIG. 2. Single cycle P-E loops as a function of measurement frequency from 1 kHz and 250, 100, and 1 Hz. The measured polarization is roughly constant, and the coercive field monotonically decreases from ~6 MV/cm at 1 kHz to ~4 MV/cm at 1 Hz, indicating modest leakage contributions and a strong frequency dependence consistent with domain nucleation and growth.

DC-voltage tests are next introduced and discussed. Figure 3(a) shows the quasistatic current–voltage (*i*–*V*) measurements of the Al,BN/*n*GaN heterostructure. The plot includes six data traces, each collected starting at zero applied volts. Trace 1 is the initial applied bias from the virgin as-deposited state, during which the bottom electrode is charged positive. The trace shows no obvious anomalies besides an

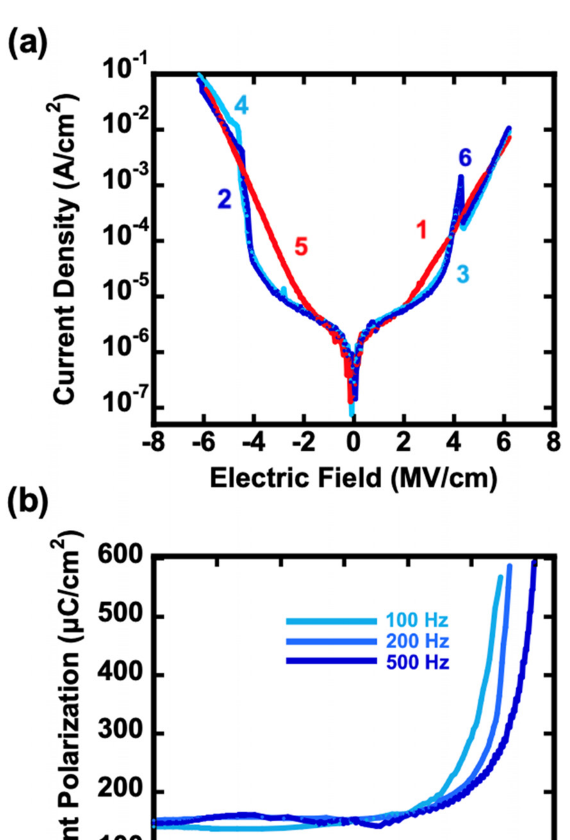

FIG. 3. (a) DC I–V curves of the Al,BN heterostructure, taken on 200 μm diameter W top electrodes. The current densities increase abruptly near 4 MV/cm and are asymmetric. The asymmetry is expected in this heterostructure with differing electrode work functions, carrier concentrations, and band alignments; (b) apparent polarization vs bipolar voltage fatigue cycles at 100, 200, and 500 Hz, and capacitors survive at least 10^7 cycles without hard breakdown. Leakage currents rise rapidly above 10^6 cycles, thus inflating the apparent polarization value.

30 April 2024 17:21:19

Published under an exclusive license by AIP Publishing

increasing current density with applied field. Trace 2 follows trace 1 with no intermediate voltage application or rest period. The bottom electrode is now negative, and the response shows a steep increase in leakage current density at ~-4 MV/cm. Trace 3 follows immediately, returning to a bottom electrode positive voltage, revealing a prominent feature at $\sim$4 MV/cm. Trace 4 continues the voltage sequence bottom electrode negative and again shows the current jump ~-4 MV/cm. Trace 5 repeats the negative voltage cycle illustrating the leakage current difference for cycles that do and do not cause switching. Finally, trace 6 shows a second positive pulse that reverses the polarization highlighting the consistency of current vs field between reversal cycles.

These measurements reveal several interesting observations: (i) the current density values are strongly asymmetric for field cycles that produce switching in the vicinity of E_c, this is not unusual for a capacitor stack with such strong chemical, work function, and carrier density contrast, including the possibility of a significant GaN accumulation/depletion zone; (ii) comparing the polarization and leakage measurements shows that strong leakage current anomalies at $\pm$4 MV/cm are close to the low frequency coercive fields, while we cannot currently assign mechanisms, it is likely that interface charge accumulation/depletion, band bending, polarization reversal, and trap filling/emptying are all possible contributors; and (iii) this system produces roughly order-of-magnitude leakage current windows separating the polarization-up and polarization-down states in both orientations. Finally, while not shown here, measurements collected from many capacitors show that the anomalies are consistent in both voltage and current density.

Figure 3(b) shows the measured polarization vs number of fatigue cycles for different measurement frequencies for the 210 nm Al,BN/GaN heterostructure. The measured polarization is relatively constant to $\sim10^5$ cycles and increases non-linearly thereafter. This increase is associated with rising leakage currents. The insulation resistance decreases at an accelerating rate to 10^7 cycles but does so without hard breakdown as reported previously by Zhu *et al.*[23] The leakage increase is suppressed for faster measurement frequencies. The absence of hard breakdown at 10^7 cycles is over two orders of magnitude improvement in fatigue behavior for Al,BN heterostructures and is the largest cycling endurance range for nitride wurtzite ferroelectrics to date, especially given the relatively low measurement frequencies. Utilizing field plates and thick metal electrodes is expected to reduce electric field crowding at electrode edges and reduce heat generation, respectively, and is expected to further improve fatigue behavior. Measurement at higher frequencies is also expected to further improve fatigue behavior. While endurance in III-N ferroelectrics needs much additional study, the improvements presented presently are an important small step toward a comprehensive structure-process-property relationship model.

Local polar orientation in as-deposited and switched Al,BN is confirmed using piezoforce microscopy (PFM). These experiments start with W dot electrodes that are woken up with ac field-cycling and then set by unipolar pulses to the +P or −P polarization states (as defined by the last voltage experienced by the bottom electrode). The samples are subsequently submerged in a 10% H_2O_2 bath at room temperature for 15 min for W removal. The previously electroded regions and their un-electroded surrounding are then PFM analyzed. Figure 4 shows PFM phase maps for capacitor locations where the final bottom electrode voltage was +V [Fig. 4(a)] and −V [Fig. 4(b)]. In both maps, a dotted white line indicates the perimeter of the initially present electrode. Figure 4(a) shows a uniform color, thus uniform phase inside and outside of the original dot capacitor area. This and the +V final-applied-voltage are consistent with an as-deposited polarization-up orientation. It is interesting that all other Al,BN films grown under similar sputtering conditions are oriented oppositely in the as-deposited state, i.e., polarization-down. The present polarization is parallel to, and likely stabilized by, the underlying GaN polarity. This indicates that the sputtered nitride propensity to grow polarization-down does not overwhelm substrate templating effects. We also note that the polar orientation inferred by PFM is consistent with the leakage current data in Fig. 3(a), i.e., switching first occurs when −V is applied to the bottom electrode. For the capacitor poled bottom electrode negative, the PFM map in Fig. 4(b) shows a uniform circular region 180° out of phase with its surroundings, separated by a smooth and abrupt boundary. This result is consistent with ferroelectric switching.

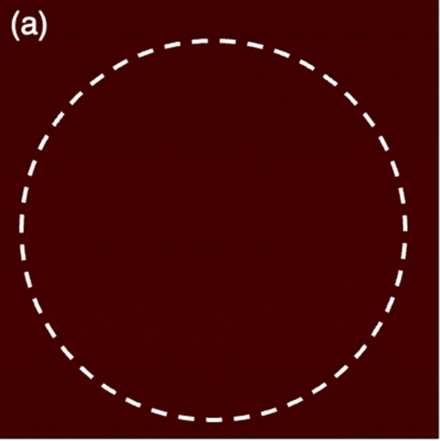

FIG. 4. PFM data on regions where the sample was previously electrically poled and the W electrode removed. (a) Phase (°) data post-coercive voltage poling, ending with a positive bias. The phase is uniform throughout the surface, with minimal difference in amplitude. (b) Phase (°) data for post-coercive voltage poling, ending with a negative bias. The phase is uniform within the electrode and changes by 180° outside the electrode.

30 April 2024 17:21:19

Published under an exclusive license by AIP Publishing

Ferroelectric behavior is experimentally observed in epitaxial Al,BN films grown on GaN at 300 °C substrate temperatures by reactive sputtering. The films exhibit uniform *c*-axis orientation, epitaxial in-plane crystallographic registry, smooth surfaces with partial step-and-terrace morphologies, and sub-nanometer rms roughness. The Al,BN films are ferroelectric, supporting a ∼125 $\mu C/cm^2$ remanent polarization that can be measured unambiguously at 1 Hz. These Al,BN capacitors survive 10^7 field cycles without hard failure but become increasingly conductive above 10^5 cycles. A combination of leakage current measurements and PFM analysis reveals an as-deposited polarization-up orientation, i.e., polarization reversal from the as-deposited state occurs with a negative voltage applied to the bottom electrode.

See the supplementary material for the tapping mode AFM images of the Al,BN heterostructures mentioned in this study.

This material is based upon work supported by the U.S. Department of Energy, Office of Science, Office of Basic Energy Sciences Energy Frontier Research Centers program under Award No. DE-SC0021118. Chloe Skidmore is supported by Army Research Office (ARO) research contract W911NF-24-1-0010 and contributed PFM imaging of the ferroelectric nitrides prepared in this study. The authors would also like to acknowledge the Penn State Materials Characterization Lab and the Penn State Nanofabrication Lab, as part of the Penn State Materials Research Institute.

AUTHOR DECLARATIONS

Conflict of Interest

The authors have no conflicts to disclose.

Author Contributions

Joseph Casamento: Conceptualization (equal); Data curation (lead); Formal analysis (lead); Investigation (lead); Methodology (lead); Resources (equal); Writing – original draft (lead); Writing – review & editing (lead). **Fan He:** Data curation (supporting); Formal analysis (supporting); Investigation (supporting); Methodology (supporting); Writing – review & editing (supporting). **Chloe Skidmore:** Investigation (supporting); Methodology (supporting); Writing – review & editing (supporting). **John Hayden:** Data curation (supporting); Investigation (supporting); Methodology (supporting); Writing – review & editing (supporting). **Josh Nordlander:** Data curation (supporting); Investigation (supporting); Methodology (supporting); Writing – review & editing (supporting). **Joan M. Redwing:** Methodology (supporting); Resources (supporting); Writing – review & editing (supporting). **Susan Trolier-McKinstry:** Funding acquisition (lead); Investigation (supporting); Project administration (supporting); Resources (supporting); Writing – review & editing (supporting). **Jon-Paul Maria:** Conceptualization (equal); Funding acquisition (lead); Investigation (supporting); Methodology (supporting); Writing – original draft (supporting); Writing – review & editing (supporting).

DATA AVAILABILITY

The data that support the findings of this study are available from the corresponding author upon reasonable request.

REFERENCES

[1] S. Fernández Garrido, G. Koblmüller, E. Calleja, and J. S. Speck, J. Appl. Phys. **104**, 033541 (2008).
[2] S. Mita, R. Collazo, A. Rice, J. Tweedie, J. Xie, R. Dalmau, and Z. Sitar, Phys. Status Solidi C **8**(7–8), 2078 (2011).
[3] A. K. Tan, N. A. Hamzah, M. A. Ahmad, S. S. Ng, and Z. Hassan, Mater. Sci. Semicond. Process. **143**, 106545 (2022).
[4] Y. Arakawa, K. Ueno, H. Imabeppu, A. Kobayashi, J. Ohta, and H. Fujioka, Appl. Phys. Lett. **110**, 042103 (2017).
[5] S. Fichtner, N. Wolff, F. Lofink, L. Kienle, and B. Wagner, J. Appl. Phys. **125**, 114103 (2019).
[6] J. Hayden, M. D. Hossain, Y. Xiong, K. Ferri, W. Zhu, M. V. Imperatore, N. Giebink, S. Trolier-McKinstry, I. Dabo, and J. P. Maria, Phys. Rev. Mater. **5**, 044412 (2021).
[7] G. Schönweger, R. Md, N. Islam, A. Wolff, L. Petraru, H. Kienle, S. Kohlstedt, and P. Fichtner, Status Solidi RRL **17**, 2200312 (2023).
[8] S. R. C. McMitchell, A. M. Walke, K. Banerjee, S. Mertens, X. Piao, M. Mao, K. Katcko, G. Vellianitis, M. Van Dal, Y. M. Lin, G. Van den Bosch, R. Delhougne, and G. S. Kar, ACS Appl. Electron. Mater. **5**, 858–864 (2023).
[9] W. Zhu, F. He, J. Hayden, Z. Fan, J. I. Yang, J. P. Maria, and S. Trolier-McKinstry, Adv. Electron. Mater. **8**, 2100931 (2022).
[10] W. Zhu, J. Hayden, F. He, J. I. Yang, P. Tipsawat, M. D. Hossain, J. P. Maria, and S. Trolier-McKinstry, Appl. Phys. Lett. **119**, 062901 (2021).
[11] K. H. Kim, I. Karpov, R. H. Olsson III, and D. Jariwala, Nat. Nanotechnol. **18**, 422 (2023).
[12] S. L. Tsai, T. Hoshii, H. Wakabayashi, K. Tsutsui, T. K. Chung, E. Y. Chang, and K. Kakushima, Jpn. J. Appl. Phys., Part 1 **61**, SJ1005 (2022).
[13] R. Guido, T. Mikolajick, U. Schroeder, and P. D. Lomenzo, Nano Lett. **23**(15), 7213 (2023).
[14] J. Kataoka, S. L. Tsai, T. Hoshii, H. Wakabayashi, K. Tsutsui, and K. Kakushima, Jpn. J. Appl. Phys., Part 1 **60**, 030907 (2021).
[15] D. Wang, P. Wang, S. Mondal, S. Mohanty, T. Ma, E. Ahmadi, and Z. Mi, Adv. Electron. Mater. **8**, 2200005 (2022).
[16] P. Wang, D. Wang, S. Mondal, and Z. Mi, Appl. Phys. Lett. **121**, 023501 (2022).
[17] P. Wang, D. Wang, N. M. Vu, T. Chiang, J. T. Heron, and Z. Mi, Appl. Phys. Lett. **118**, 223504 (2021).
[18] J. Casamento, K. Nomoto, T. S. Nguyen, H. Lee, C. Savant, L. Li, A. Hickman, T. Maeda, J. Encomendero, V. Gund, A. Lal, J. C. M. Hwang, H. G. Xing, and D. Jena, in *IEEE International Electron Devices Meeting (IEDM)* (IEEE, San Francisco, CA, 2022), pp. 11.1.1–11.1.4.
[19] G. Schönweger, A. Petraru, M. Islam, N. Wolff, B. Haas, A. Hammud, C. Koch, L. Kienle, H. Kohlstedt, and S. Fichtner, Adv. Funct. Mater. **32**, 2109632 (2022).
[20] M. Islam, G. Schönweger, N. Wolff, A. Petraru, H. Kohlstedt, S. Fichtner, and L. Kienle, ACS Appl. Mater. Interfaces **15**, 41606 (2023).
[21] P. M. Reimer, H. Zabel, C. P. Flynn, J. A. Dura, and K. Ritley, Z. Phys. Chem. **181**, 375 (1993).
[22] K. Yazawa, J. Hayden, J. P. Maria, W. Zhu, S. Trolier-McKinstry, A. Zakutayev, and G. L. Brennecka, Mater. Horiz. **10**, 2936 (2023).
[23] W. Zhu, F. He, J. Hayden, Q. Tran, J. I. Yang, P. Tipsawat, B. Foley, T. N. Jackson, J. P. Maria, and S. Trolier-McKinstry, "Unique ferroelectric fatigue behavior and exceptional high temperature retention in $Al_{0.93}B_{0.07}N$ films," arXiv:2208.06486 (2022).

30 April 2024 17:21:19

Published under an exclusive license by AIP Publishing